Supplemental material

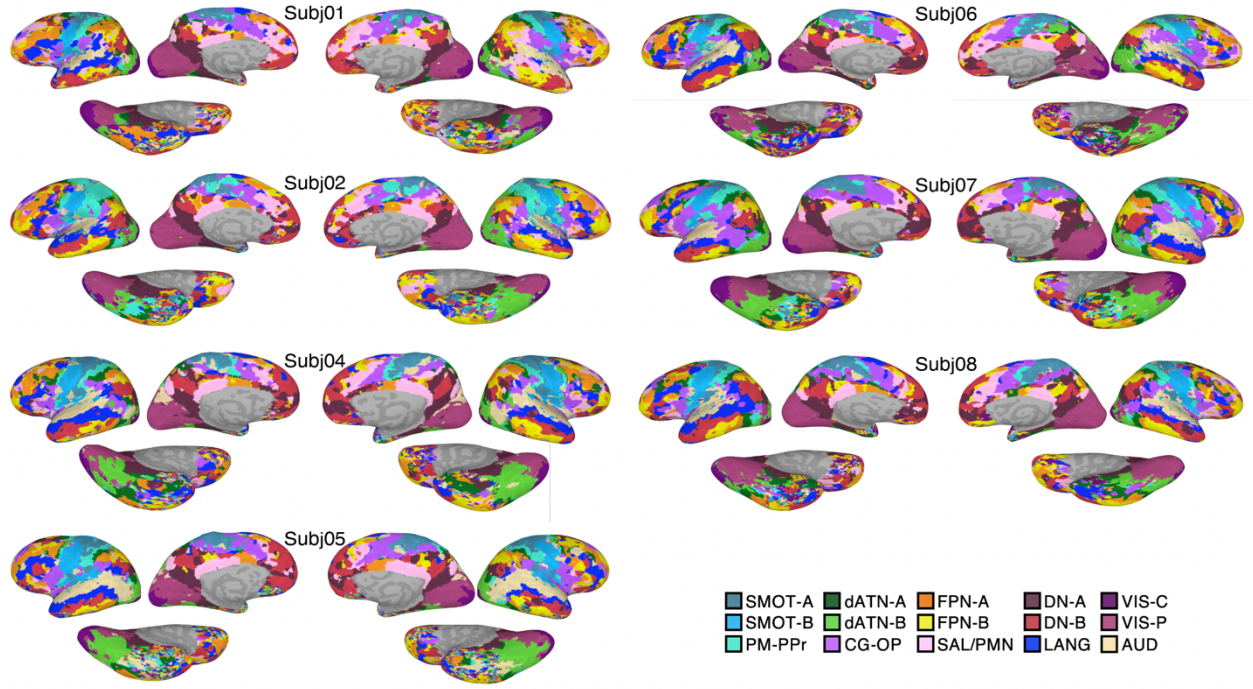

Fig S1. Cortical network parcellations for individual participants. Networks were parcellated based on the Yeo HCP 15-network parcellation[33] using the multi-session hierarchical Bayesian model (MS-HBM) method[32].

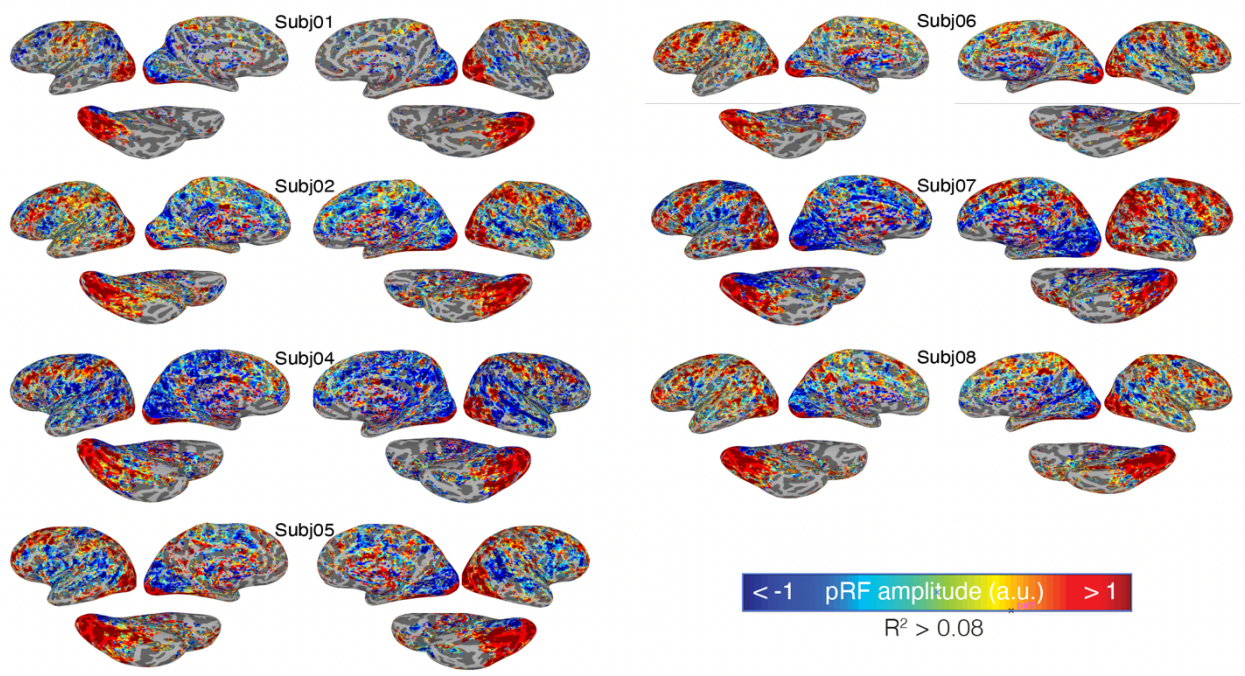

Fig S2. PRF amplitude maps from all participants. Only voxels with greater than 8% variance explained by the pRF model are shown.

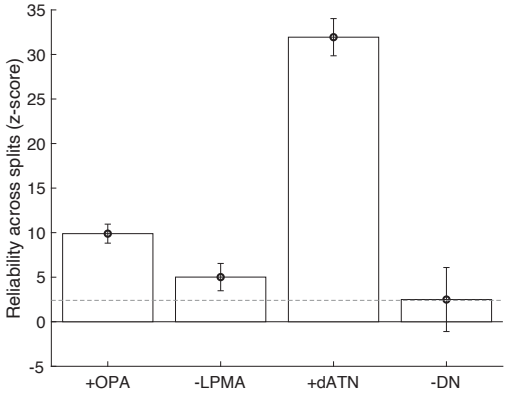

Fig S3. Reliable fitting of pRF amplitude in OPA and LPMA, dATN, and DN. To assess the reliability amplitude (i.e., positive versus negative), we iteratively compared the amplitude of significant pRFs from individual runs of pRF data. We fit our pRF model on each individual run of pRF data. Vertices were binarized according to significance and amplitude – for +pRF reliability in OPA, significant vertices with a positive amplitude were assigned to 1, all other vertices 0; for -pRF reliability in LPMA, the opposite was done: significant negative amplitude vertices were assigned a value of 1, and all other vertices set to 0.

After binarization, for each pair of pRF runs (e.g., run 1 v run 2), we calculated the dice coefficient within each ROI between two retinotopy runs, for each participant. For each participant, this resulted in 3 "observed" dice coefficients. The average of the 3 observed values was compared against a null distribution to evaluate the significance of each pRF amplitude's run-to-run consistency. To establish the null distributions, we performed 1000 randomly shuffled iterations with equal proportion of significant voxels for each run pairing (resulting in 3000 bootstrapped values representing the distribution of dice coefficients expected by chance).

The average dice co-efficient for amplitude exceeded the 99th percentile compared to shuffled data in all regions of interest, suggesting pRF amplitudes were reliable. Importantly, because of the noise inherent to any single run of fMRI data, this reliability assessment represents a very conservative measure of reliability. Bars represent mean reliability versus shuffled distribution across participants. Error bars represent standard error across participants.

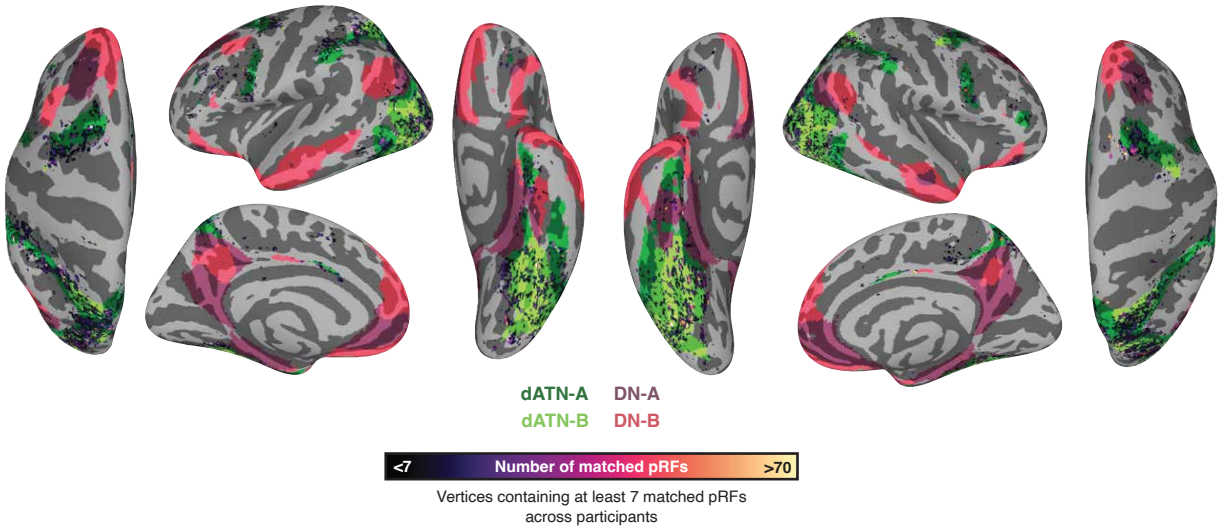

Fig. S4. Spatial distribution of +dATN pRFs matched with -DN pRFs in cortex across all participants. Vertices are colored based on number of matched pRFs. Only vertices with greater than 7 matched pRFs (i.e., at least one for each subject) are shown. Yeo 2015 network maps[33] dATN A-B and DN A-B are shown for reference. Note that pRFs were matched in individualized dATN of each participant and are not expected to correspond precisely with the group network maps.

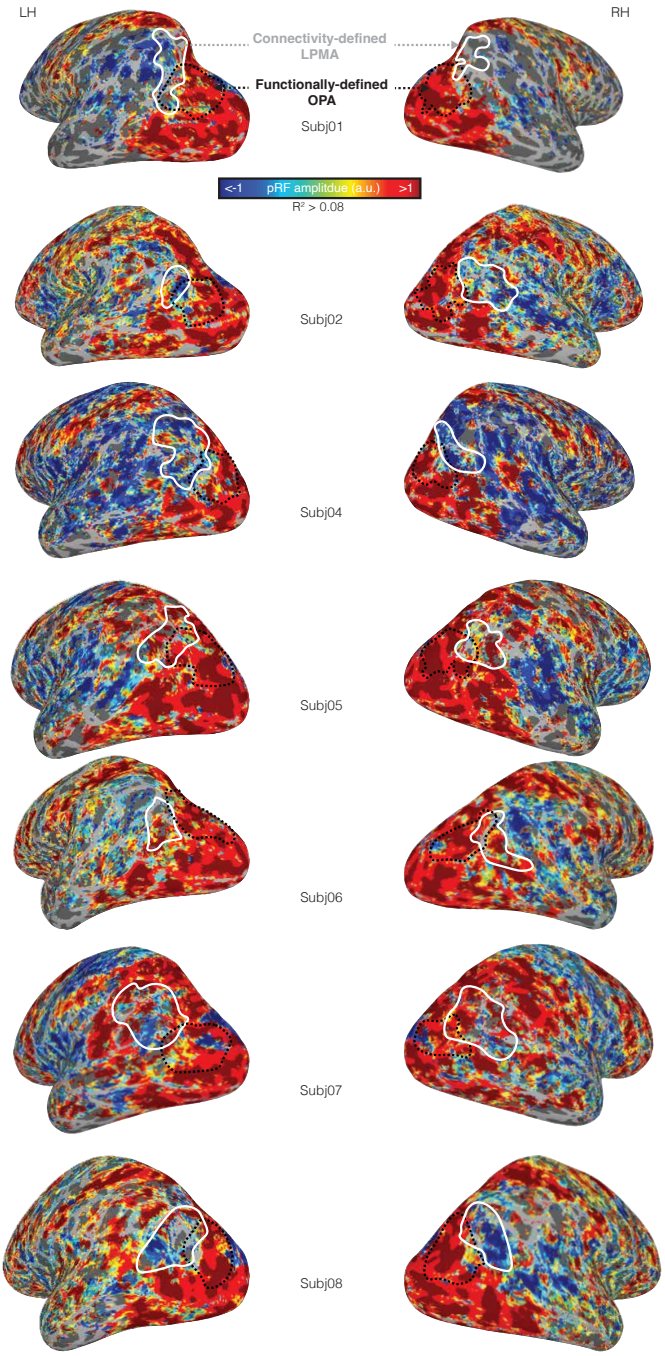

Fig S5. All participants OPA/LPMA and pRF amplitude.

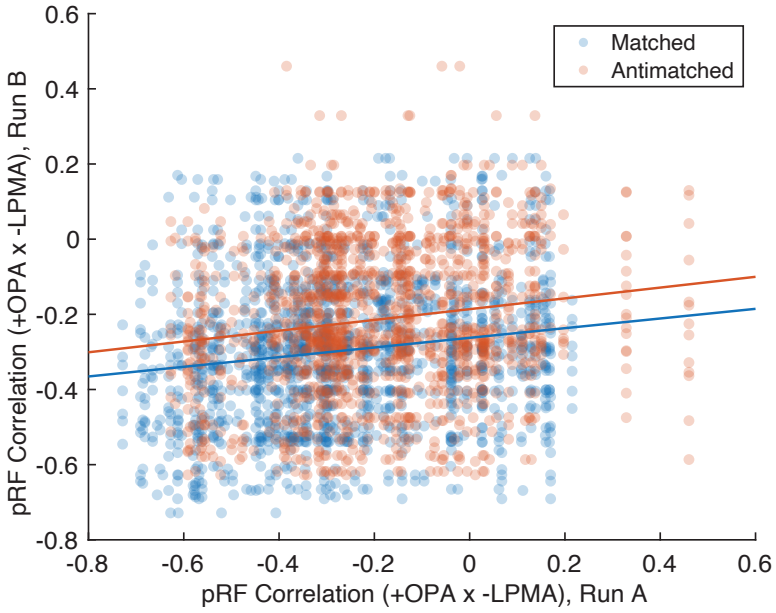

Fig S6. Matched and anti-matched pRFs correlation values reliability did not differ. One potential issue when comparing matched and antimatched pRF populations is that the antimatched population might be more variable in the strength of their correlation compared with matched pRFs. We confirmed this was not the case by examining the correlation between the matched and antimatched pRF time series for each pair of resting-state runs independently. We then tested the correlation in these run-to-run pairs. We found no difference in run-to-run reliability between matched and antimatched pRFs (matched pRFs: r = 0.1502, antimatched pRFs: r = 0.1510; difference: z = 0.0225, p = 0.98).

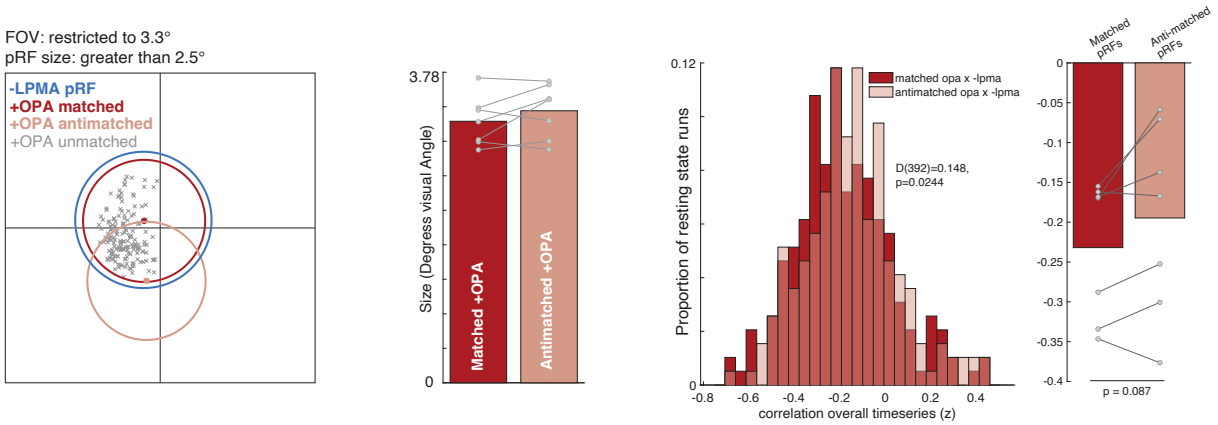

Fig. S7. Retinotopic coding structures the interaction at rest when matched and antimatched pRFs are matched for center position and size. Left. Because of the differential distribution of receptive field centers across eccentricities, antimatched +OPA pRFs could be more likely to be eccentric and larger than matched pRFs. To ensure that this did not influence our results, we repeated the pRF matching analysis between -LPMA and +OPA with a restricted field of view (all pRFs within 3.3°) and size (all pRFs larger than 2.5°). Center. Using these constraints, both matched and antimatched pRFs were matched for size. Right. Histogram shows the correlation of the average -LMPA and +OPA matched (dark red) and antimatched (light red) time series for each resting state run in all participants. These distritbutions were significantly different (D(392)=0.148, p=0.0244). Bars show the average correlation value across resting-state runs between -LPMA and +OPA matched and antimached pRFs for each participant. Matched pRFs had a stronger negative correlation compared to antimatched pRFs (t(6)=2.03, p=0.087; 5/7 participants).

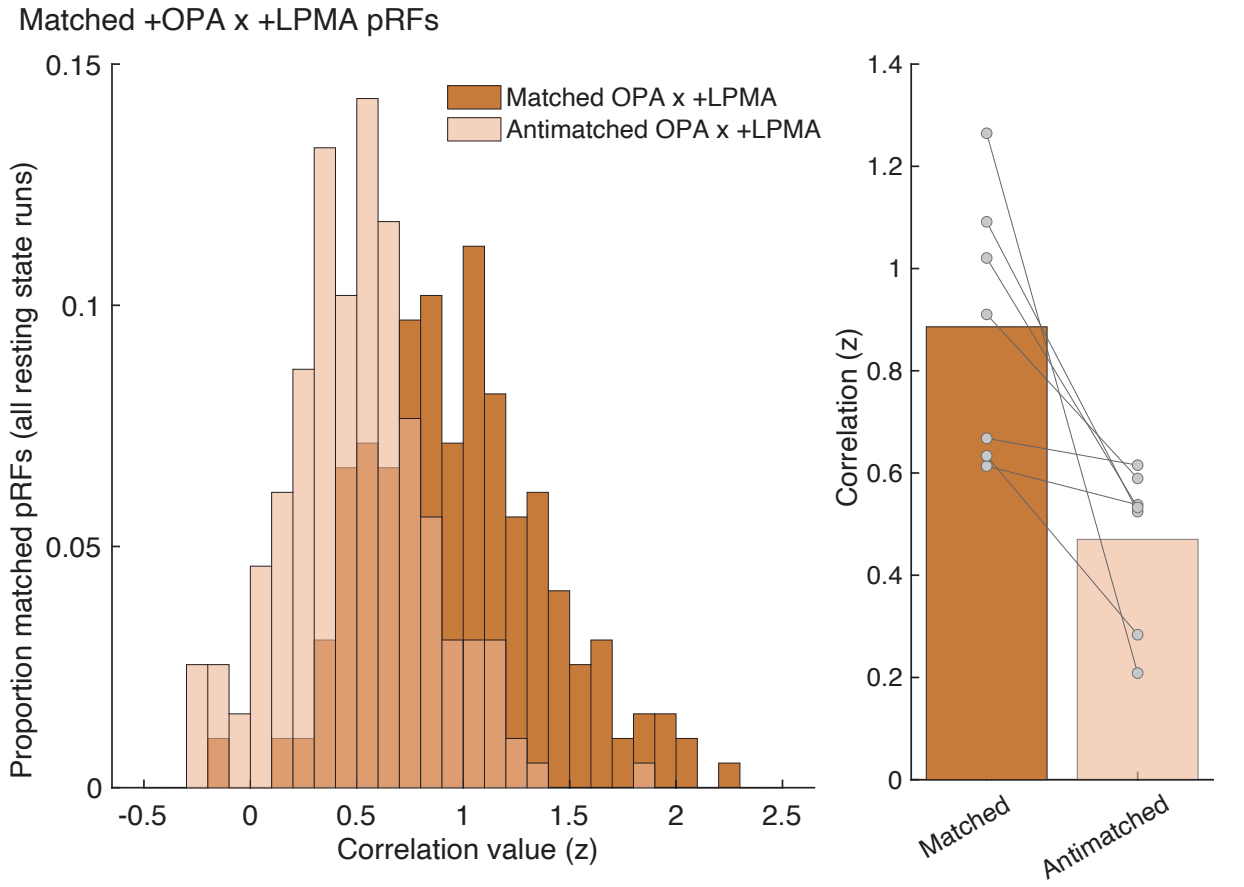

Fig. S8. Retinotopic specific co-fluctuation of +pRFs in OPA and LPMA. We matched LPMA and OPA based on their center position estimates. We evaluated the correlation between +LPMA pRFs and the correlation of the matched and antimatched time series using the same procedure as -LPMA pRFs (see methods). Left. Histogram shows the correlation of the average +LMPA and +OPA matched (dark orange) and antimatched (light orange) time series for each resting state run in all participants. Right. Average correlation value across resting-state runs between -LPMA and +OPA matched and antimached pRFs for each participant. Matched pRFs had significantly stronger negative correlation compared to antimatched pRFs ($t(6)=3.22$, $p=0.018$). This is consistent with retinotopic coding structuring the interaction between +pRFs in perception and memory areas, and that these +pRFs are positively correlated, even during rest.

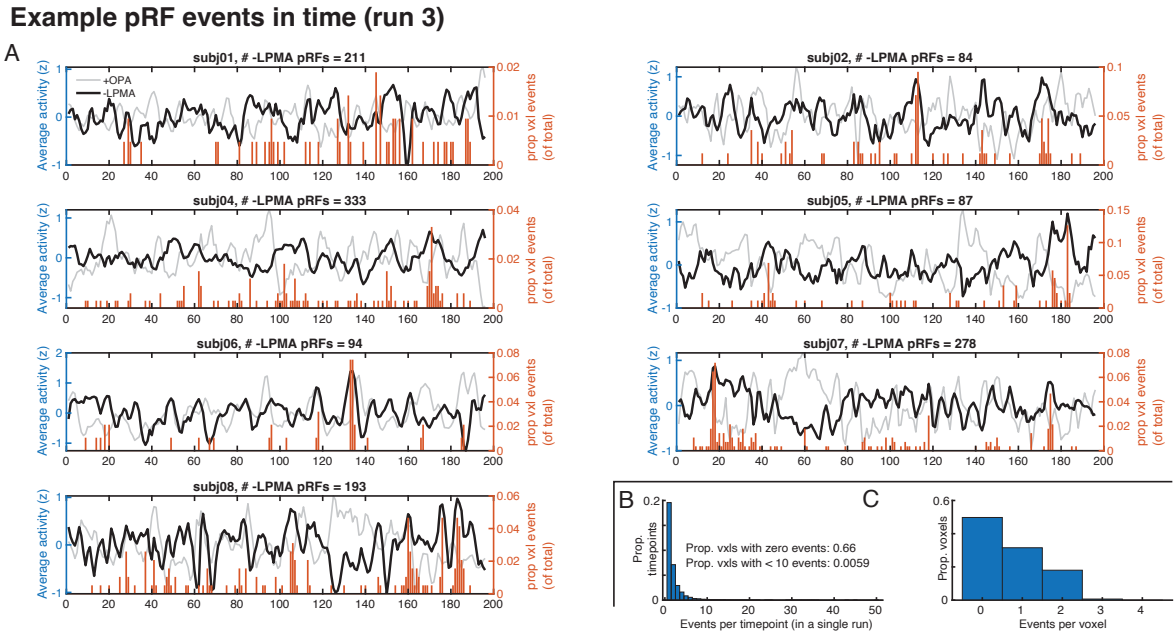

Fig. S9. Events are widely distributed in time. A. Example time series from each participant (each individual's third resting-state session). Thick black line shows the -LPMA pRFs average time series, grey line shows average +OPA pRFs time series. Orange bars show the proportion of voxels within each ROI with events at a given time point. Events (time points where individual voxel time series exceeds z-score of 2.4) are widely distributed in time, with relatively few voxels (<15%) in each ROI exhibiting simultaneous events. This suggests that, after preprocessing, time series from individual voxels were effectively isolated. B. Number of events per time point combined for top down and bottom up events. Bars indicate the number of voxel events detected at a given time point within a resting-state run, aggregated across runs. Events were sparsely distributed: most time points contained no events (Proportion = 0.66, bar not shown), with the number of events decreasing approximately exponentially. This is further evidence for a wide temporal distribution of events. C. Proportion of voxels with events in each run. No voxel had more than 4 events per run. Data are combined between top down and bottom-up events.

Supplemental methods and results

Comparison of matched pRFs versus randomly sample pRF pairs

One possibility is that the bottom 10 pRFs are a non-representative set of pRFs within an area. To control for this possibility, we implemented an alternative analysis method to compare the influence of retinotopic coding on voxel-scale pull-pull dynamics. For this analysis, we established the pairwise distances between all pRF centers across two regions (e.g., +OPA and -LPMA pRFS). Then, for each pRF, we randomly sampled 10 pRFs from the top 33% of distances (the top 1/3 furthest pRF pairs) and calculated the average correlation between these randomly matched pRF pairs. We considered the top 33% because the overwhelming majority of pRFs constituted relatively equal "good" matches. This resulted in 1000 correlation values for each pRF. Then, for each pRF. we compared the mean correlation from these 1000 iterations with the correlation of the top 10 best matched pRFs. We then averaged the matched and random pRF values from each participant and compared matched versus random pRFs using a paired t-test.

Importantly, because some of the randomly sampled "poorly matched" pRFs constituted "good matches" for other pRFs, for this analysis we computed the correlation of the matched/random pRF timeseries for each pRF separately. Importantly, because the values were computed for each pRF separately, the correlation values are lower than the main text analysis where all pRF timeseries in a region were averaged together before computing the correlation value.

Consistent with our main analysis, we found that retinotopic coding underpinned the opponent dynamic between the -DN and +dATN ($t(6)=8.43$, $p<0.001$) and -LPMA and +OPA pRFs ($t(6)=3.012$, $p=0.024$). On the other hand, retinotopic coding did not influence the interplay between -LPMA and OFA ($t(6)=0.59$, $p=0.57$) and -LPMA and FFA ($t(6)=2.01$, $p=0.09$). These results support the overall conclusions in our manuscript using the matched versus anti-matched analysis.

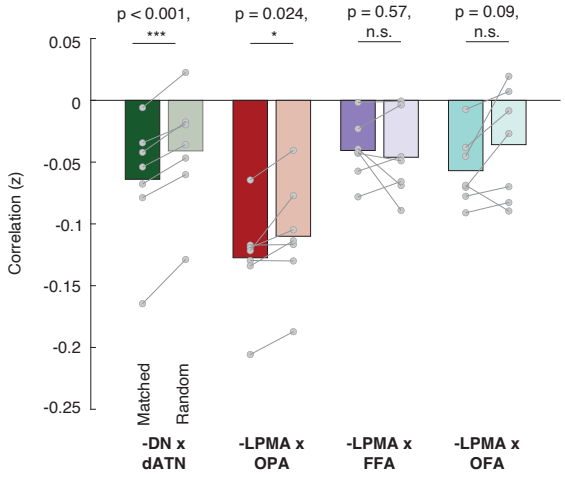

Fig. S10. Comparison of matched versus randomly-paired pRFs.